Horizontal spatial gradient sounding and geomagnetic depth sounding in the period range of daily variations

Ulrich Schmucker

Geophysikalisches Institut Goettingen

1 Basic concepts

The long-standing but not so frequently used alternatives to magneto-tellurics (*MT*) are the various types of magneto-variational (*MV*) soundings. They provide the only trustworthy information about in-situ conductivities at great depth when applied to such long-periodic variations as daily variations (*S*) and smoothed storm-time variations (*Dst*). These global variation fields cover the period range from a few hours to many days, and their depths of penetration extend from about 300 *km* to 1000 *km*. MT impedance estimates for long-periodic variations are difficult to obtain, not counting the increasingly dominating distortions at most sites, which are caused by the tangential-magnetic (TM) modes in the electric field. Provided the external source field is an electromagnetic field in the tangential-electric (TE) mode, a standard assumption for frequencies below 1 *Hz,* the same applies to its observable magnetic field above ground, and as a consequence MV responses become less and less influenced by local near-surface anomalies of conductivity when periods and penetration depths increase. But this gives rise to a different problem for MV sounding, connected to the then dual cause for observable variations of the vertical magnetic component (B_z) in the following sense.

MV response estimates are based on the time-series analysis of geomagnetic variations in all three components. Unless global estimates are sought from internal to external potential ratios, the locally observed vertical B_z -variations are set in relation to those of the horizontal components (B_x , B_y), for a given frequency, either to these components themselves or to their spatial derivatives with respect to the horizontal coordinates *x* and *y,* or to both. Conventional *geomagnetic depth sounding* (*GDS*) proceeds from a linear relation of the form $B_z = aB_x + bB_y$ under the assumption that the sole cause for B_z -variations are local deviations from a layered conductivity structure, leading to *induction anomalies* in the internal part of the variation field. But the stated supposition for GDS becomes less and less tenable when with increasing periods the penetration depth approaches the lateral dimensions of the external source field, for example their half-width. The result are B_z -variations in the absence of induction anomalies. The 1-dimensional MV sounding method to be applied then is the horizontal spatial gradient (*HSG*) method, henceforth referred to as *gradient sounding* for short. Its basic relation in terms of the C-response of the thus assumed layered structure is $B_z = C(\omega)\,\{\partial B_x/\partial x + \partial B_y/\partial y\}$, with $Z(\omega) = i\omega\, C(\omega)$ as scalar MT impedance of the structure. It should be realized that starting with daily variations the observed B_z -variations reflect mainly spatial non-uniformities of the source rather than the presence of induction anomalies, as in the case of less deeply penetrating short periodic variations such as bay-type variations around 1 *cph* outside jet-regions.

The combination of both methods obviously requires a distinction between the normal part of the variation field, as it would be observed in the absence of induction anomalies, and its superimposed anomalous part, where such anomalies exist. Henceforth these two parts are denoted with the subscripts *n* and *a*, respectively, for example $B_z = B_{nz} + B_{az}$. Because the

anomalous parts represent a potential field of exclusively internal origin, in contrast to the normal part of external *and* internal origin, its vertical and horizontal components can be converted into each other within the range of the respective induction anomaly, a possibility which could be utilized for a physically founded separation. As a substitute normal and anomalous parts of the horizontal components will be separated by fitting polynomials to B_x and B_y within a network of observing sites, either as functions of time or frequency-by-frequency. Using low-order polynomials their synthesis smoothes out localized anomalies and thereby should provide good approximations for B_{nx} and B_{ny} at any given site within the network. Similarly differentiation of the polynomials yields their spatially smoothed derivatives $\partial B_{nx}/\partial x,\ldots$. The normal part B_{nz} of the vertical components represents then that part of the observed B_z-variations, which can be correlated to the stated spatial derivatives, while any remaining anomalous part is connected linearly to B_{nx} and B_{ny} by definition.

The thus reformulated basic equations for separate gradient sounding and GDS are

$$B_{nz} = C(\omega)\{\partial B_{nx}/\partial x + \partial B_{ny}/\partial y\} + \delta B_{nz} \tag{1}$$

and

$$B_{az} = z_H B_{nx} + z_D B_{ny} + \delta B_{az}\,, \tag{2}$$

respectively, which restores the GDS transfer functions z_H and z_D in their original definitions (Schmucker, 1970; Section 3.8). These equations represent univariate and bivariate linear regression problems, to be solved toward their respective transfer functions by least squares. Combining them leads to the trivariate problem

$$B_z = C(\omega)\,\{\partial B_{nx}/\partial x + \partial B_{ny}/\partial y\} + z_H B_{nx} + z_D B_{ny} + \delta B_z \tag{3}$$

for joint gradient sounding and GDS. In the thereby assumed presence of lateral non-uniformities in the substructure, obviously the use of a scalar C-response represents an approximation. For consistency it is replaced by a thereby introduced tensor C-response in correspondence to the tensor impedance for MT sounding. Its elements are denoted accordingly as $C_{xx}, C_{xy},..$, and their relations to the elements of the TE-mode MT impedance are $Z_{xx}^{(TE)} = i\omega\, C_{xx}$, $Z_{xy}^{(TE)} = i\omega\, C_{xy}$, .. by definition.

Involving then all three independent spatial derivatives, with $\partial B_x/\partial y = \partial B_y/\partial x$ for potential fields, two more terms have to be added to the right-hand-side of eq. (3). The resulting multivariate expression is given the special form

$$B_z = C_1\,\{\partial B_{nx}/\partial x + \partial B_{ny}/\partial y\} + C_2\,\{\partial B_{ny}/\partial y - \partial B_{nx}/\partial x\} + C_3\,\partial B_x/\partial y + z_H B_{nx} + z_D B_{ny} + \delta B_z \tag{4}$$

with five transfer functions to be determined:

$$C_1 = (C_{xy} - C_{yx})/2\,,\ C_2 = (C_{xy} + C_{yx})/2\,,\ C_3 = (C_{xx} - C_{yy}) \tag{5}$$

for the normal part of B_z and

$$z_H = \frac{\partial C_{xx}}{\partial y} - \frac{\partial C_{yx}}{\partial x}, \quad z_H = \frac{\partial C_{xx}}{\partial y} - \frac{\partial C_{yx}}{\partial x} \tag{6}$$

for its anomalous part. Details about the derivations of the eqs (1) to (6) can be found in a forthcoming publication, here also in their extension to spherical coordinates.

The implications of the three generalized C-responses are as follows: C_1 represents the invariant equivalent to the Berdichevsky-average for the tensor MT impedance, C_2 accounts for the C-response anisotropy and C_3 for 3D-effects, provided no rotated coordinates can be found for with C_3 vanishes. The invariant sum of the diagonal elements cannot be determined, a consequence of a missing fourth independent derivative. The GDS transfer functions for the anomalous part, finally, turn out to express the spatial derivatives of the tensor C-response elements, indicating in which direction the depth of penetration varies in response to laterally changing conductivities.

2 Data processing

The time series which have been analysed consist of the hourly mean values of two years 1964-65, published in the yearbooks of 30 observatories in Europe and brought on punched cards under the supervision of Dr. Winch. The observatories are spread more or less evenly over the continent up to 60 degrees in geomagnetic latitude. This limit has been set to avoid complications due to the Polar Electrojet further north. With a sampling rate of one value per hour and thereby a Nyquist frequency of 12 cycles per hour (*cpd*), the frequency range of response estimates with reliable phases ends at 6 *cpd* or 8 *cpd* at the most. As a consequence no detailed information can be expected about upper mantle conductivities above 200 km depth, as it is evident also in the $\rho^* - z^*$ plots of Fig. 1.

The spectral analysis toward estimates of transfer functions is carried out separately for the quasi-periodic *regular* daily variations (S_r) and their spectral continuum background (S_{cont}) due to transient *irregular* variations in connection to magnetic storm-time activity. For S_r a harmonic analysis is performed from midnight to midnight in Universal time on selected days, leading for each analysed day and frequency to event spectra in the form of un-smoothed Fourier products. They extend in frequency from 1 *cpd* to 6 *cpd*. In the analysis of S_{cont} harmonics are derived for the 72 time-section of *T=10* days lengths, which can be fitted into the two years of data without overlap. The resulting Fourier products are band-averaged with Parzen filters within eight frequency bands of constant width $\Delta f = 1 cpd$. Their mid-frequencies begin at 0.5 cpd and end at 7.5 cpd , with $T\Delta f = 10$ Fourier products within each band.

Because the time series have been high-pass filtered prior to the harmonic analysis, with a cut-off at 0.5 *cpd,* contributions are largely excluded from the Equatorial Ring Current (*ERC*) in the *Dst* recovery phase of magnetic storms. This would have been necessary in any case for the intended combination of gradient sounding and GDS. Because this recovery phase is well described by a single spherical harmonic $P_1(\cos\vartheta)$, a linear relation would arise between the horizontal component and its derivative with respect to geomagnetic latitude ϑ, which inhibits

a least squares solution of eq. (3). In addition the Sq-variations of the respective months have been subtracted hour-by-hour from the high-pass filtered time series.

In the concluding step of data processing spectral estimates are derived by a weighted summation over the event spectra. If *K* denotes the number of transfer functions to be determined, the cross- and power-spectra of the input variables define the $K \times K$ *spectral matrix* which has to be inverted for least squares estimates. With increasing number *K*, however, this matrix may become ill-conditioned for inversion. The ultimate cause are linear dependencies among the input variables, expressed by the squared coherencies $coh^2_{k\ell}$ for the input variables X_k and X_ℓ. For *K*=2 only one coherency matters and the possibility that the spectral matrix may be ill-conditioned is usually ignored, when analysing bivariate expressions like eq. (2). For *K*=3 as in eq. (3) already three coherencies are involved, but an eigen-value analysis of the spectral matrix has shown that its condition number is still within safe limits for an unaided inversion. Increasing the number to K=5 as in eq. (4) and now with ten coherencies among input variables, the condition number turns out to be too large for an unaided inversion without regularisation.

3 Gradient sounding results

The required spatial gradients $\partial B_{nx}/\partial x$ and $\partial B_{ny}/\partial y$ are derived by the differentiation of second order polynomials in x and y , fitted to B_x and B_y at 30 European observatories, 28 of them with usable B_z-records for gradient sounding. They are split into two groups of 14 observatories each according to their either central or marginal position within the network of sites (cf. map in Fig. 3). The resulting C-responses are presented in complex planes with $\mathrm{Re}\{C(\omega)\}$ plotted as z^*-depths downward and with the positive-valued $-\mathrm{Im}\{C(\omega)\}$ along the abscissa on a logarithmic scale. Because the arguments of the C-responses lie almost exclusively between zero and $-\pi/4$, corresponding to a phase of the MT impedance between 45 and 90 degrees, the imaginary parts are converted into apparent resistivities $\rho^* = 2\omega\mu_0 \mathrm{Im}\{C(\omega)\}^2$ for a uniform substitute half-space of resistivity ρ^*, which lies below a non-conducting top layer of thickness $\mathrm{Re}\{C(\omega)\} + \mathrm{Im}\{C(\omega)\}$.

Fig. 1 contains three $\rho^* - z^*$ plots to display the C-responses for the 14 observatories in central positions, obtained at each site for the eight frequencies of the continuum analysis. Error bars indicate confidence limits at the 68 percent probability level, and in the key for the symbols frequencies have been converted into periods in hours, for convenience. The first display to the left presents the results of an univariate regression, evaluating eq. (1) with B_z in place of B_{nz}. For the three longest periods the respective 14 estimates form clearly separated clusters. The deepest cluster between 600 *km* and 800 *km* for the 48 *hrs* period, with ρ^*-values between $1\Omega m$ and $2\Omega m$, indicates that these very long-periodic irregular variations have reached the well conducting Earth's mantle below 600 km depth.

The next following cluster for 16 *hrs* moves upwards by nearly 100 *km* . The concurrent rise to $\rho^* = 10\Omega m$ shows that these responses are already in the transition region to a more resistive mantle from 600 *km* upwards. This rise continues with further decreasing periods and levels off around $50\Omega m$, with the most shallow z^*-depths ending at 200 *km*. The resulting

depth-profile of apparent ρ^*-resistivities agrees well with global sounding results for daily variations obtained with the potential method (cf. Schmucker,1999; Table 8). The overall impression is that within the investigated depth range the resistivity structure beneath central Europe appears to be laterally quite uniform and in good agreement with what is known about deep resistivities on a global scale. It should be noted, however, that the cited global sounding results have been obtained with data from 70 to 90 globally distributed observatories, of with more than one third were in Europe.

Noting that the scatter among estimates exceeds their error limits quite frequently, we consider the possibility that this scatter is actually due to superimposed anomalous parts on the locally observed B_z. This possibility has been ignored so far. In the initial step of an iterative procedure a mean response $< C(\omega) >$ is determined by adding the spectra of all 14 sites, leading in $B_{nz} = < C(\omega) > \{\partial B_{nx} / \partial x + \partial B_{ny} / \partial y\}$ to a first approximation for the normal vertical component. Subtraction from B_z yields its anomalous part B_{az} for a bivariate least squares analysis towards the GDS transfer functions z_H and z_D according to eq. (2). By subtracting subsequently the resulting $B_{az} = z_H B_{nx} + z_D B_{ny}$ from B_z, a possibly improved approximation follows for B_{nz}, and with it the univariate least squares analysis is repeated toward new C-responses, which have been corrected for the local influence of induction anomalies. They are displayed in the second $\rho^* - z^*$ plot in the centre of Fig.1 .

As to be expected, these estimates produce much more closely clustered $\rho^* - z^*$ values than before, but they could be biased toward the mean responses used to define B_{az}. For a test C-responses are determined once more, this time simultaneously with the GDS transfer functions in a trivariate regression analysis according to eq. (3). The resulting third $\rho^* - z^*$ plot on the right shows a clearly reduced scatter, in particular for the short periods, when compared to the first plot on the left. On the other hand, not the same closeness of estimates has been achieved as in the central plot, i.e. a certain degree of bias seems to exist when deriving C-responses with the described iterative procedure. It does not invalidate the overall conclusion, however, that the scattered response estimates do not reflect merely inaccurate determinations, but that their scatter can be accounted for by the influence of localized induction anomalies. This will be considered in more detail in Section 4.

Fig. 2 repeats the comparison of directly and iteratively derived C-responses for the 14 observatories along the margins of the European network, now based on the analysis of daily variations on 124 quiet days in 1965-65. Because this group contains numerous observatories in Western Europe not too far from the deep Atlantic ocean, an increased scatter among the response estimates can be expected due to coast effects. This is indeed the case, as seen in the $\rho^* - z^*$ plot on the left, but as evident from the plot on the right, the removal of the anomalous parts in the same manner as before reduces this scatter effectively. Moreover, the resulting ρ^* depth-profile for the mantle fits well to the depth-profile of Fig. 1 for the continuum and observatories in central Europe, indicating a unified deep structure beneath the entire continent south of the excluded auroral zone.

4 Geomagnetic depth sounding results

So far induction anomalies have been used merely as a tool to improve C-response estimates by removing their influence on the locally observed B_z -variations. Now we turn our attention to these anomalies themselves, testing the spatial consistency of GDS transfer functions in the environment of such anomalies, also in respect to physically meaningful phases and consistent dependencies on frequency. For this purpose z_H and z_D are displayed on maps in the form of *induction vectors* for a given period. For the real or in-phase vectors $\underline{c}_{\mathrm{Re}}$ the Parkinson convention is used with a reversal of signs, for the imaginary or out-of-phase vectors $\underline{c}_{\mathrm{Im}}$ the Wiese convention (cf. Schmucker, 1970; Section 3.10). With $\underline{\hat{x}}$ and $\underline{\hat{y}}$ as unit vectors towards north and east, respectively,

$$\underline{c}_{\mathrm{Re}} = -\mathrm{Re}\{z_H\}\,\underline{\hat{x}} - \mathrm{Re}\{z_D\}\,\underline{\hat{y}} \quad \text{and} \quad \underline{c}_{\mathrm{Im}} = \mathrm{Im}\{z_H\}\,\underline{\hat{x}} + \mathrm{Im}\{z_D\}\,\underline{\hat{y}} \ . \tag{7}$$

We obtain with these definitions better distinguishable in-phase and out-of-phase vectors, when real and imaginary parts have the same sign, as it is characteristic at long periods. In particular near elongated anomalies they point conveniently in opposite directions, $\underline{c}_{\mathrm{Re}}$ pointing in the direction of decreasing depths of penetration toward better conducing zones and $\underline{c}_{\mathrm{Im}}$ pointing in the direction of increasing depths of penetration toward more resistive zones (cf. eq. 6).

Fig. 3 shows the thus defined induction vectors for the third frequency band of the continuum analysis. Error ellipses at the origin indicate the confidence limits in x and y direction at again the 68 percent probability level. So far not much is known, whether for periods of almost 10 hours induction anomalies might be still recognizable, recalling that the greater part of the observed B_z -variations arises from source field non-uniformities, even near coastlines. The well resolved induction vectors at numerous sites in Fig. 3 prove that this is possible, even though the lengths of the vectors are quite small except at coastal sites. Here the observatories VAL in Ireland and COI in Portugal show typical coast effects for more less straight continental margins, with the two vectors in opposite directions and perpendicular to the coastline. Both have about the same lengths, implying a substantial phase of B_{az} against the horizontal components of the normal field, as to be expected for long periods. Noteworthy are the deviating directions at ALM in Southern Spain, pointing in their real parts towards the Mediterranean Sea. Within the continent induction vectors barely reach 0.1 in lengths except at a few exceptional sites like RSV near Copenhagen or WNG near Hamburg, in both cases with opposing vectors for the real and imaginary parts, as it should be.

For a mutual test the same GDS transfer functions have been derived in two different ways. The display at the top contains those from a bivariate regression analysis according to eq. (2), after subtracting the normal part of B_z with the aid of mean responses, now for all 28 sites, as described in Section 3. The display at the bottom refers to GDS transfer functions obtained directly from the observed B_z by means of a trivariate regression analysis according to eq. (3). The good agreement demonstrates that comparable results evolve whether a beforehand determined constant mean response is used to define B_{nz} or a concurrently determined and thus variable local C-response.

Figs 4 and 5 continue with the display of induction vectors, adding those for the next three continuum frequencies. They are shown separately for the southern and the central European

segments of the observatory network. The covered period range extends from about ten to four hours, corresponding to frequencies from 2.5 *cpd* to 5.5 *cpd,* and thus connects to the periods at which GDS results for sub-storm variations set in. In Fig. 4 we note a consistent pattern of induction vectors along the Mediterranean Sea and its adjacent countries, from ALM and EBR at the Spanish coast to AQU near Rome, GCK in Jugoslavia, and PAG in Bulgaria. Their directions and phases are quite stable for all periods and the real vectors seem to point to a concentration of induction currents in or below the western part of the Mediterranean sea between Spain and Morocco. It appears to be unlikely that an isolated system of eddy currents could have been set up in the Mediterranean Sea itself in view of the long periods involved. Instead it seems that globally induced currents in the oceans seep into it from the east and west, following possibly conductive conduits, where they have to cross continents, or globally induced currents at greater depth are drawn into a highly conductive substructure under the Mediterranean Sea. Noting that the induction vectors at the Spanish inland observatory TOL (Toledo) are already nearly within error limits, a very shallow conductor has to be involved in any case.

Fig. 5 provides a closer view of the inland induction anomalies in central Europe for the same periods. Again consistent patterns of induction vectors can be followed up through all periods. On the profile from RSV to DOU in Belgium they indicate the presence of a well conducting slab in north-westerly direction with its centre below WIT in Holland, where the anomalous B_{az} disappears, with opposing induction vectors to the northeast (RSV, WNG) and the southwest (DOU). The same anomaly seems to be visible further to the southeast at NGK near Berlin and perhaps even at PRU near Prague, both observatories at the south-western margin of the conductor similar to DOU. At RSV and WNG. where the GDS transfer functions are most prominent, the expected change of phases with periods is clearly seen, starting at the ten hour period with dominating imaginary parts and phases close to 90 degrees, ending at four hours with both parts of comparable size and thus phases of about 45 degrees.

A connection to the extensively studied North-German-Polish anomaly of bay-type disturbances is very likely, even though the strike of this anomaly is east-west and thus somewhat different. The only other central European observatory with a clearly resolved and consistent anomaly is LVV in Galicia, which almost certainly can be brought in connection to the Carpathian induction anomaly of bay-disturbances. Very conspicuous is the absence of any significant anomaly in the quadrangle of FUR near Munich, WIK near Vienna, HRB near Bratislava and THY at Lake Balaton. The overall impression is that the thus outlined and relatively weak inland anomalies are real phenomena and not artefacts of the complicated combination of 1-dimensional gradient sounding with multi-dimensional GDS, which is necessary for induction studies with long-periodic variations. This view is strengthened by the good agreement with the independently obtained but not shown GDS results for daily variations.

References

Schmucker, U., 1970. Anomalies of geomagnetic variations in the Southwestern United States. *Bull. Scripps Institution of Oceanography*, vol. **13**, University of California.

Schmucker, U., 1999. A spherical harmonic analysis of solar daily variations in the years 1964-65: response estimates and soured fields for global induction – II. Results. *Geophys. J. Int*., **136**, 455-476.

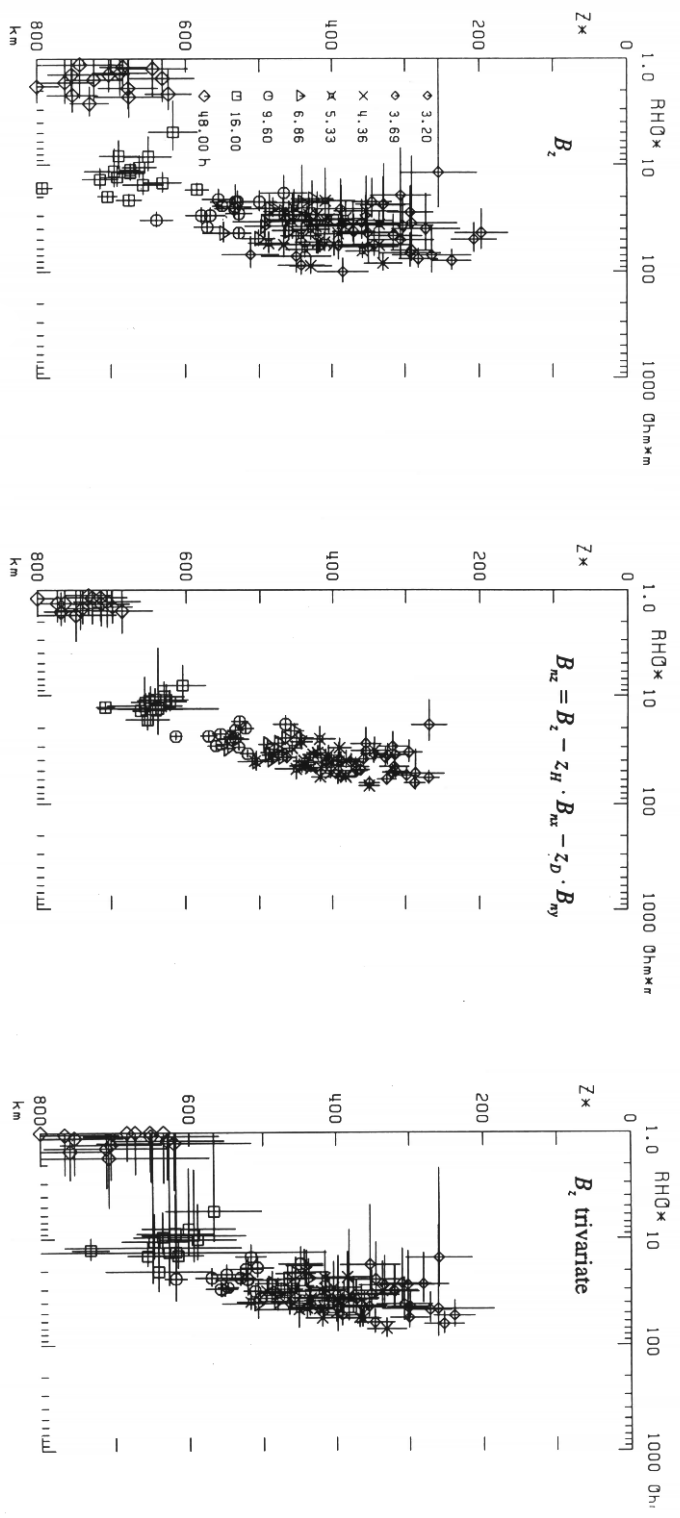
Geomagnetic gradient sounding with S-continuum at 14 obs. in central Europe
B_z
$B_{nz} = B_z - z_H \cdot B_{nx} - z_D \cdot B_{ny}$
B_z trivariate
RHO*
Ohm*m
Z*
km
3.20
3.69
4.36
5.33
6.86
9.60
16.00
48.00 h

Fig. 1

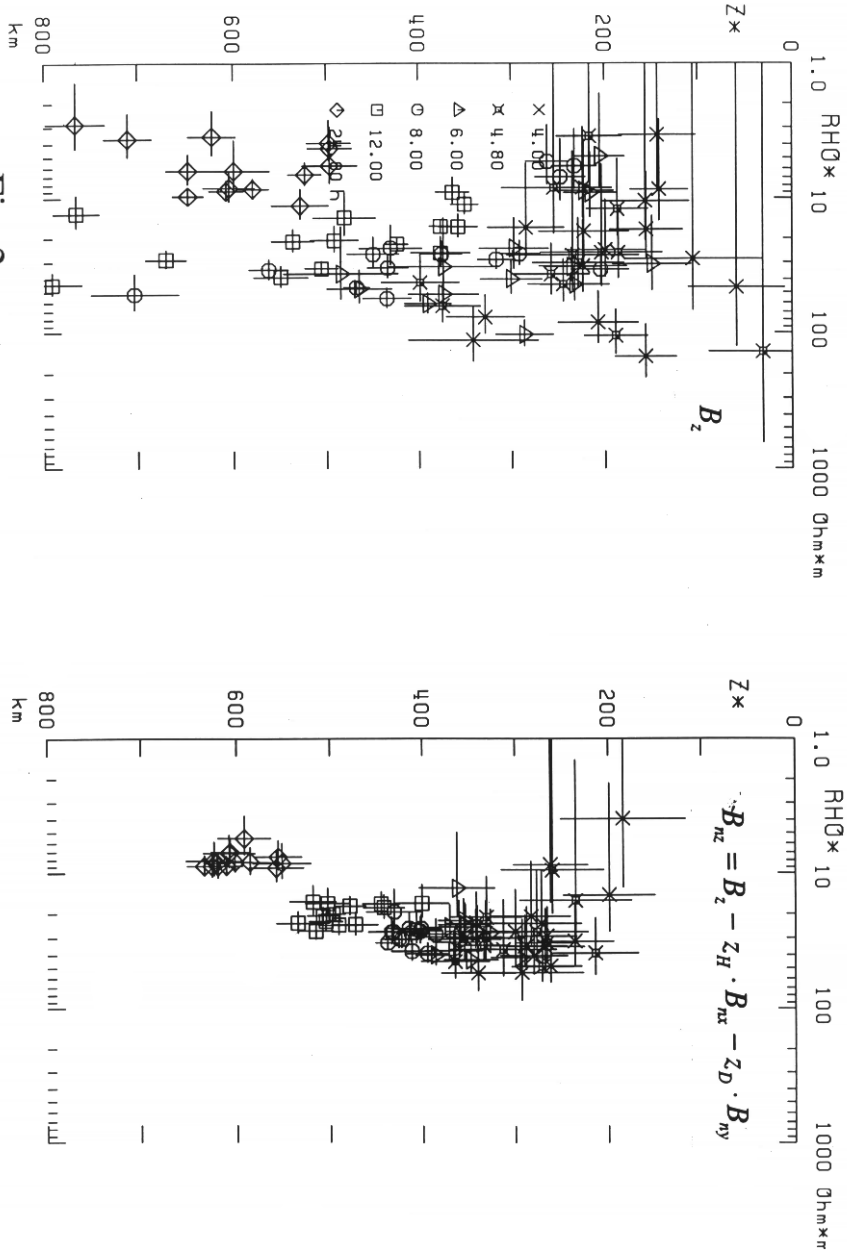
Geomagnetic gradient sounding with S-harmonics at 14 obs.in marginal Europe
Z*
RHO*
Ohm*m
B_z
$B_{nz} = B_z - z_H \cdot B_{nx} - z_D \cdot B_{ny}$
km
4.00
4.80
6.00
8.00
12.00

Fig. 2

Geomagnetic depth sounding with S-continuum

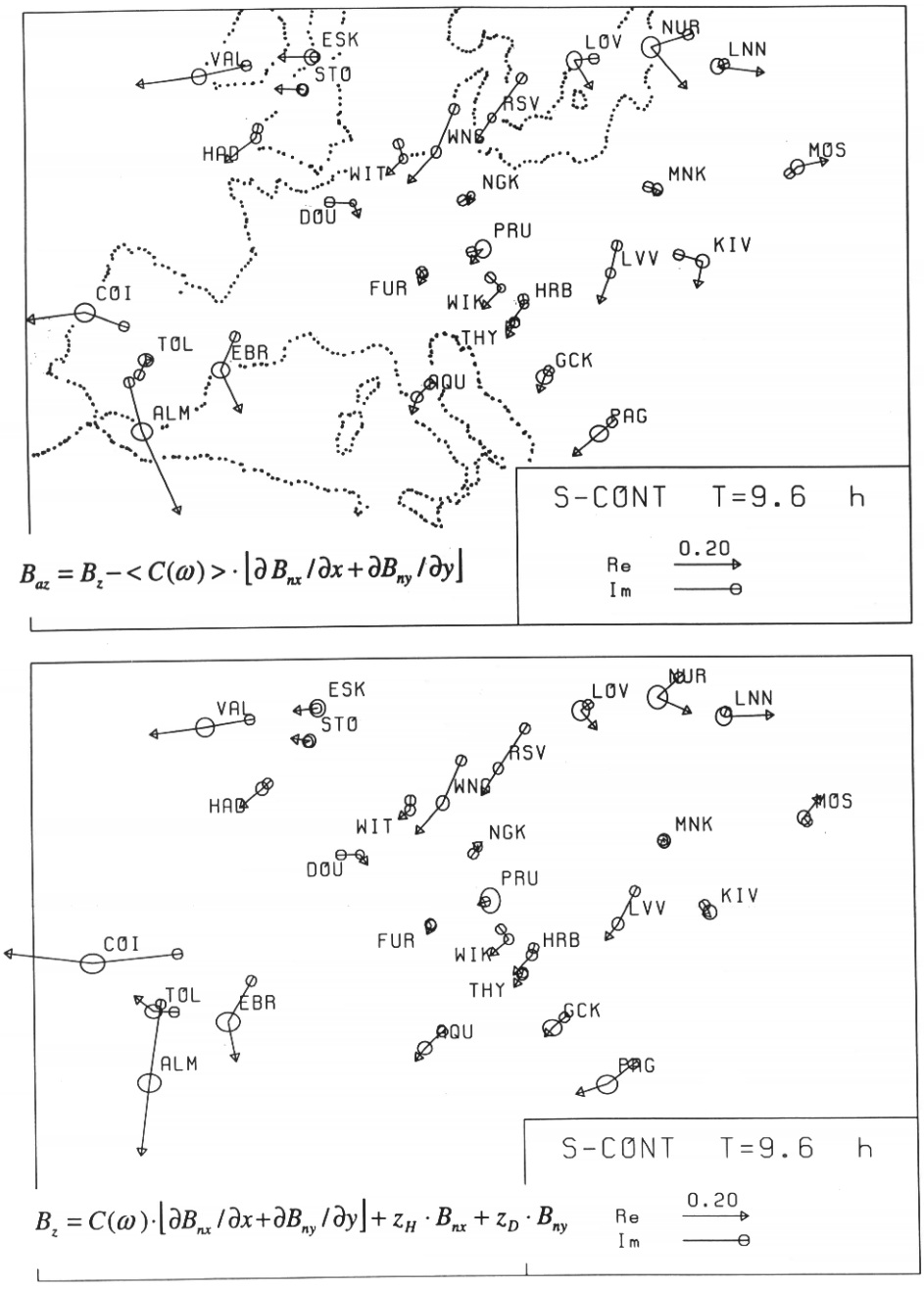

Fig. 3

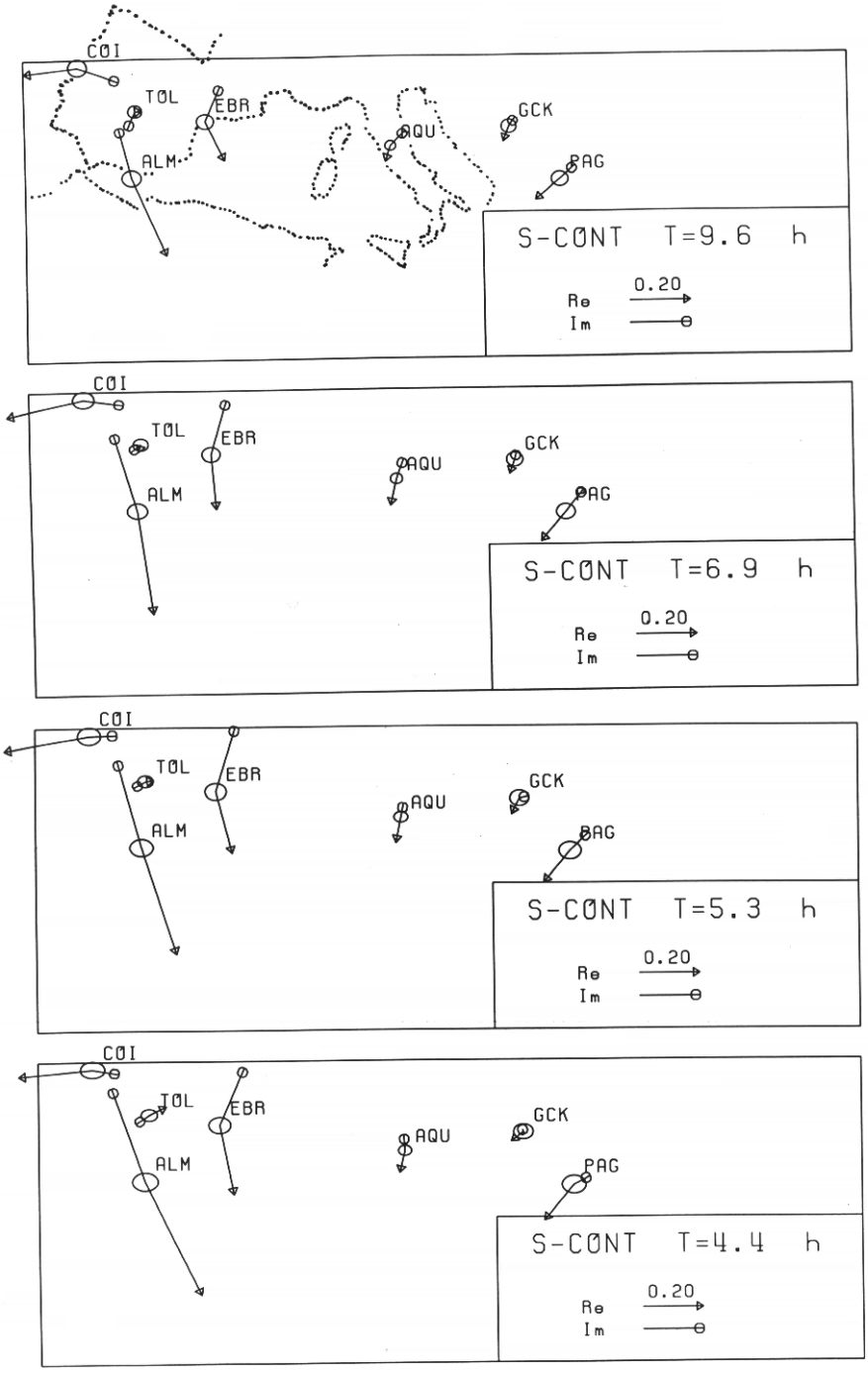
COI
TOL
EBR
ALM
AQU
GCK
PAG
S-CONT T=9.6 h
Re 0.20
Im
COI
TOL
EBR
ALM
AQU
GCK
PAG
S-CONT T=6.9 h
Re 0.20
Im
COI
TOL
EBR
ALM
AQU
GCK
PAG
S-CONT T=5.3 h
Re 0.20
Im
COI
TOL
EBR
ALM
AQU
GCK
PAG
S-CONT T=4.4 h
Re 0.20
Im

Fig. 4

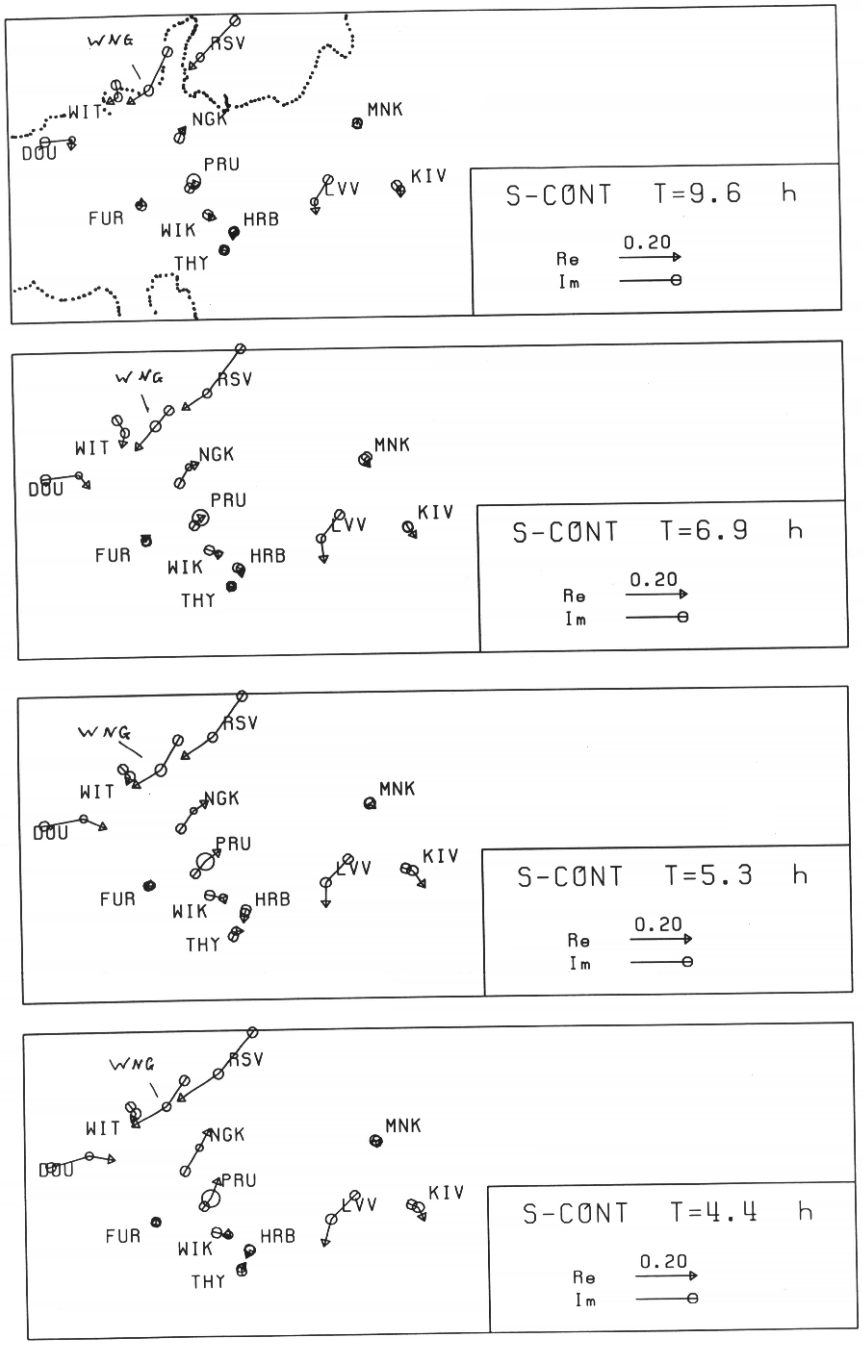
WNG
RSV
WIT
NGK
MNK
DOU
PRU
LVV
KIV
FUR
WIK
HRB
THY
S-CONT T=9.6 h
Re 0.20
Im
S-CONT T=6.9 h
S-CONT T=5.3 h
S-CONT T=4.4 h

Fig.5